IEEE Access
Multidisciplinary ⋮ Rapid Review ⋮ Open Access Journal

Received February 26, 2020, accepted March 10, 2020, date of publication March 17, 2020, date of current version April 1, 2020.

Digital Object Identifier 10.1109/ACCESS.2020.2981393

A Review of Broadband Low-Cost and High-Gain Low-Terahertz Antennas for Wireless Communications Applications

RUI XU[1], STEVEN GAO[1], BENITO SANZ IZQUIERDO[1], CHAO GU[2], PATRICK REYNAERT[3], (Senior Member, IEEE), ALEXANDER STANDAERT[3], (Student Member, IEEE), GREGORY J. GIBBONS[4], WOLFGANG BÖSCH[5], (Fellow, IEEE), MICHAEL ERNST GADRINGER[5], (Member, IEEE), AND DONG LI[6]

[1]School of Engineering and Digital Arts, University of Kent, Canterbury CT2 7NZ, U.K.
[2]Centre for Wireless Innovation, Queen's University Belfast, Belfast BT7 1NN, U.K.
[3]Department of Electrical Engineering, Katholieke Universiteit Leuven, 3000 Leuven, Belgium
[4]International Manufacturing Centre, WMG, The University of Warwick, Coventry CV4 7AL, U.K.
[5]Microwave and Photonic Engineering, Graz University of Technology, 8010 Graz, Austria
[6]CAST, Xi'an Institute of Space Radio Technology, Xi'an 710061, China

Corresponding authors: Rui Xu (rxuilj@163.com) and Steven Gao (s.gao@kent.ac.uk)

This work was supported in part by the CHIST ERA WISDOM Project through EPSRC under Grant EP/P015840/1, in part by the EPSRC under Grant EP/S005625/1 and Grant EP/N032497/1, and in part by the EPSRC HVM Catapult Fellowship Scheme under Grant REF: EP/L017121/1.

ABSTRACT Low-terahertz (Low-THz, 100 GHz-1.0 THz) technology is expected to provide unprecedented data rates in future generations of wireless system such as the 6th generation (6G) mobile communication system. Increasing the carrier frequencies from millimeter wave to THz is a potential solution to guarantee the transmission rate and channel capacity. Due to the large transmission loss of Low-THz wave in free space, it is particularly urgent to design high-gain antennas to compensate the additional path loss, and to overcome the power limitation of Low-THz source. Recently, with the continuous updating and progress of additive manufacturing (AM) and 3D printing (3DP) technology, antennas with complicated structures can now be easily manufactured with high precision and low cost. In the first part, this paper demonstrates different approaches of recent development on wideband and high gain sub-millimeter-wave and Low-THz antennas as well as their fabrication technologies. In addition, the performances of the state-of-the-art wideband and high-gain antennas are presented. A comparison among these reported antennas is summarized and discussed. In the second part, one case study of a broadband high-gain antenna at 300 GHz is introduced, which is an all-metal model based on the Fabry–Perot cavity (FPC) theory. The proposed FPC antenna is very suitable for manufacturing using AM technology, which provides a low-cost, reliable solution for emerging THz applications.

INDEX TERMS Antennas, low-terahertz, additive manufacturing (AM), high gain, Fabry–Perot cavity (FPC), low-cost, three-dimensional printing (3DP).

I. INTRODUCTION

A. DEFINITION OF LOW-TERAHERTZ (LOW-THz)

Generally, the conventional terahertz (THz) [1]–[3] wave refers to an electromagnetic (EM) wave with a frequency in the range of 0.1 to 10.0 THz (wavelength of 3.0 mm to 30.0 μm), which coincides with the millimeter wave in the long wavelength band and the infrared light in the short wavelength band. However, there are very few research results and data related to the terahertz band, which is mainly limited by effective terahertz generation sources and sensitive detectors, so this band is also called the THz gap [4], [5]. With the development of a series of new technologies and new materials in the 1980s, especially the development of

The associate editor coordinating the review of this manuscript and approving it for publication was Kwok L. Chung.

ultra-fast technology, obtaining broadband stable pulsed THz sources has become a quasi-conventional technology. In the past few decades, some works have been conducted at low-terahertz (Low-THz) band [6], [7], which spectrum refers to the portion of electromagnetic (EM) spectrum from 100 GHz to 1 THz, and the corresponding wavelength is from 3.0 mm to 0.3 mm. In Low-THz band, the equipment requirements are not as high as high-THz requirements, and it maintains many characteristics of THz wave. Therefore, Low-THZ has become a hot research field.

B. THE APPLICATION OF LOW-THz ANTENNA

Because of the unique and huge advantages of THz wave, it is considered as the optimal choice for a new generation of imaging systems. Like conventional imaging technologies at microwave or millimeter wavebands, THz imaging technology also adopts THz rays to illuminate the object to obtain information of the sample through the transmission or reflection of the object. What's more, imaging with higher resolution [8]–[11] can also be achieved by increasing the frequencies and bandwidth of incident waves. With this function, THz imaging is rapidly developed to meet the requirement of some commercial applications, such as THz medical imaging test [12]–[14], atmospheric and environmental monitoring [15]–[17], THz radar [18], [19], national security and anti-terrorism [20]–[23].

Since the data rate of mobile communication systems has been growing exponentially over the past few decades, substantial work has been done in this field. Previously, have been extensively applied for its unprecedented data rates, especially in the existing fifth generation (5G) wireless communication systems [24]–[27]. In addition, higher data rates are also required to serve the dramatically increase of wireless data traffic in the near future. To address this issue, wireless communication devices can carry more signals at THz band, which provide a potential solution to guarantee the transmission rate and channel capacity. In particular, technologies in Low-THz band are of great significance to the upcoming beyond-5G or 6G communication system [28]–[30]. Furthermore, technologies in THz band have an unparalleled advantage in space communications [31]–[33]. Because it is in a state of near vacuum in outer space, it is not necessary to take the influence of moisture into consideration. In this case, the message transmission rate is several hundred to one thousand times faster than current that of ultra-wideband technology, which allows THz communications to perform highly secure satellite communications with extremely high bandwidth.

Among all the communication systems, antennas are the most fundamental components, which take the responsibility of receiving and transmitting EM waves. Due to the large transmission loss [34]–[36] of Low-THz waves in free space, it is urgent to design a very high gain Low-THz antenna to compensate for additional path loss, thereby increasing the distance of the THz communication system and overcoming the power limitation of THz source generator [37]–[39]. Due to the lack of efficient THz transmitting antennas and sources, it cannot yet be commercialized in the communication field recently.

C. MANUFACTURING OF LOW-THz ANTENNAS

With the continuous development of processing technologies, many new technologies have able to meet the processing requirements of Low-THz and the processing cost is greatly reduced. Additive manufacturing (AM) or three-dimensional printing (3DP) [40]–[43] is a technique for constructing objects by printing them layer by layer, based on a digital model file, using glutable materials such as powdered metal or plastic. 3DP is very suitable for structural parts of large size and complex shape. The precision of the 3D printing equipment can reach 0.01mm, but the powder metallurgy parts need to be sintered after being printed and formed. The shrinkage rate and high temperature deformation exist in sintering. High-precision parts still need to be fabricated with machining methods. Many manufacturing methods, such as computer numerical control (CNC) machining, electrical discharge machining (EDM), low-temperature co-fired ceramic (LTCC), and Printed circuit board (PCB), are able to meet the high precision processing requirements of different electronic devices or products.

Except for the processing technologies, new materials are also important for the processing and design of THz antennas. For insurance, graphene [44], [45] has a resistivity of only about $10^{-6}\Omega\cdot$cm, which is lower than that of copper or silver. It is currently the smallest resistivity material in the world. Due to its extremely low resistivity and the fast movement of electrons, it is expected to be used to develop a new generation of thinner, faster conductive electronic components. Nowadays, graphene has been used to design reconfigurable circuits or antennas [46]–[49] with its superconducting properties. On the basis of the emergence of new processing technologies and new materials, the research on Low-THz antennas has become more practical and meaningful.

This paper aims to provide a detailed review of recent development on Low-THz wideband and high gain antenna that utilizes different ways with corresponding manufacturing processes. Furthermore, a novel wideband high gain RCA is designed at 300 GHz. Scaled model is fabricated using AM and measured in anechoic chamber. Measurement results are discussed and compared to the simulation results, followed by conclusions in Section IV.

II. REVIEW OF WIDEBAND HIGH-GAIN LOW-THz ANTENNAS

To design Low-THz high gain antenna, some methods have been demonstrated. Up to date, many papers have been published on this topic, such as horn antennas [50]–[51], traditional planar antenna arrays [52]–[56], transmit-arrays (TA) or lens antennas [57]–[63], reflect-arrays (RA)[64]–[70], and resonant cavity antennas (RCA) [71]–[83].

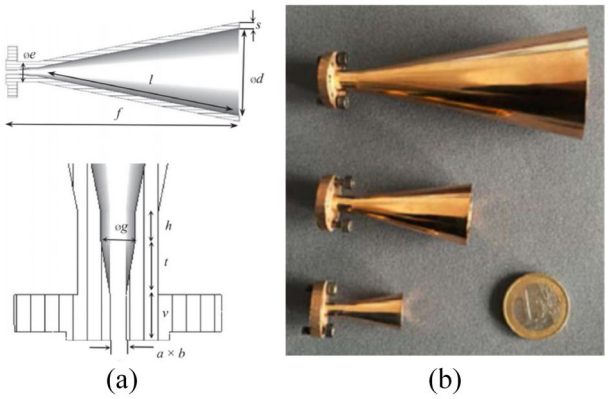

FIGURE 1. Conical horns fabricated by SLM Cu-15Sn in [50]: (a) overall view and the zoomed-view of the flange and rectangular-to-circular waveguide taper, and (b) photograph from the top: E–, D–, and H-band horns.

A. HORN ANTENNAS

The horn antenna is a widely used antenna, which has the advantages of simple structure, wide frequency bandwidth, and large power capacity. A reasonable horn size allows for good radiation performances, such as a fairly sharp main lobe, small side lobes and a high gain.

In Fig. 1 [50], three horns are printed by selective laser melting (SLM) Cu-15Sn 3DP technology. Balancing between the cost and the antenna performance, the manually polished Cu–15Sn is selected to develop a series of conical horn antennas at the E-band (60–90 GHz), D-band (110–170 GHz), and H-band (220–325 GHz). The waveguide interface on the flange is milled for better flatness. As a result, the measured antennas' impedance bandwidth ($|S_{11}| < -20$ dB) covers the completely operational band. The observed in-band gain are more than 22.5, 22.0, and 21.5 dB for the E-, D-, and H-band antennas, respectively. There exists a 0.5 dB difference between the simulated and measured gain at these three frequency bands.

Another 300-GHz step-profiled pyramid horn antenna is investigated on a LTCC multi-layer substrate [51]. Through drilling cavities with gradually expanding size on each layer, the shape of horn is formed which inherently has a stepped profile as shown in Fig. 2 (a). The dielectric layers are parallel to H plane in conventional dielectric loaded H-plane sectoral SIW horn antenna, which may lead to mismatching between the edge of the dielectric slab and air, and decreasing the operational bandwidth. In addition, the increase of dielectric and conductor loss in THz band will degrade the antenna efficiency. To overcome these issues, vertical SIW hollow structure formed by drilling cavities and metallic vias in stacked LTCC layers is proposed in this paper. Compared with H-plane SIW structure, the vertical SIW offers better antenna gain and symmetric radiation patterns in both E-plane and H-plane owing to flexibility in aperture design. Multiple metallic vias design effectively reduces the leakage of EM wave between vias and metal layers. The vertically formed hollow structure can be fabricated without

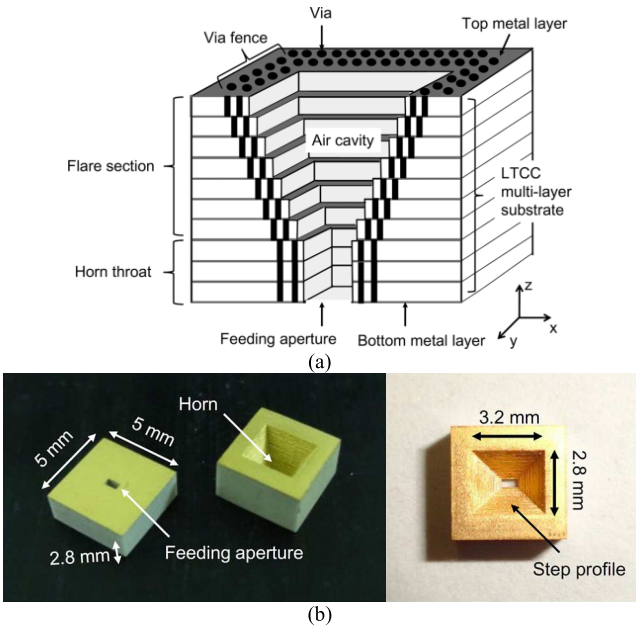

FIGURE 2. Schematic view of LTCC horn antenna in [51]; (b) side view and top view of fabricated LTCC horn antenna.

any special fabrication process. Experimental results show that the antenna has a peak gain of 18 dBi and 100 GHz working bandwidth from 230 to 330 GHz ($|S_{11}| < -10$ dB). Measured hollow LTCC waveguide insertion loss is 0.6 dB/mm, which is low enough to be applicable to 300GHz band.

B. PLANAR WAVEGUIDE ARRAYS

Planar waveguide array has been greatly developed since the middle of the last century. Because of its unique features such as easy control of the amplitude distribution in the antenna aperture surface, high utilization of the aperture surface, small volume, and easy realization of low or very low side lobes, it has been widely used in various fields like ground, ship-borne, airborne, and navigation.

In [52], a broadband high gain corporate-feed waveguide slot array with cavities is proposed using diffusion bonding technology for 120 GHz application. The wide bandwidth characteristic is achieved by the dual-resonance caused by slot self-resonance and external mutual coupling. An outer cavity structure is employed in the 4×4 element array for each radiating slot to adjust the mutual coupling, which enables all radiating elements to have similar characteristics in the array. As a result, high gain and efficiency are achieved over a broad bandwidth.

The multilayer slot array antenna is composed of feeding network in the bottom layer and radiating waveguide in the top layer, which is hard to fabricate using conventional technology such as machining or die-casting in 120 GHz band. Eventually, diffusion bonding of laminated thin metal plates is selected for the fabrication of the proposed multilayer antenna, which has the advantage of high accuracy (± 20 um) and low loss characteristics in high frequency.

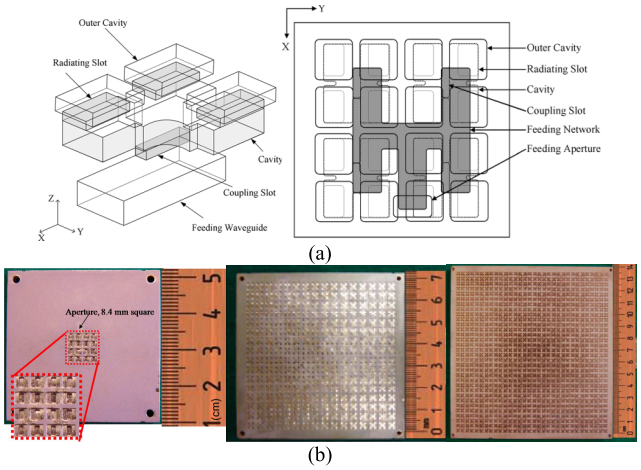

FIGURE 3. Waveguide slot antenna array in [52], [53]: (a) 2 × 2-element subarray and 4 × 4 element array; (b) Fabricated 4 × 4, 16 × 16 and 32 × 32 corporate-feed waveguide slot array.

It could also provide perfect electrical contacts between etched metal plates. The measured gain and efficiency is 21.1 dBi and 80.0% respectively. Furthermore, the 1dB-down gain bandwidth is 17.6%. Two larger-size slot arrays (16 × 16, 32 × 32) of the same structure are presented in [53], which show higher gain of 38.0 dBi and 43.0 dBi. The fabrication of even larger and more complex structure would be difficult as the metal plates with large and complex patterns are easily deformed under high pressure and temperature during the fabrication process.

Deep reactive ion etching (DRIE) process is explored for the fabrication of a corporate-feed slotted waveguide array antenna in [54]. The 16 × 16 array is constituted by five silicon plates (M1 to M5) as shown in Fig. 4 (a), which forms the corporate feeding network and radiating part. Standard rectangular waveguide WR-3 is used to feed the array through a coupling slot etched in M1. The feeding network, which distributes the coupled power equally, is etched in M2. The cavities in M4 excites radiating slots etched in M5. For 350 GHz band, etching accuracy of thin silicon plates is critical to antenna performance. To solve the requirement for accuracy, DRIE process with etching accuracy of lower than ±5 um is developed for the fabrication process. After etching, the plates are gold-sputtered and bonded with diffusion bonding process by applying high pressure with high temperature. The top and side views of the fabricated antenna prototype are shown in Fig. 4 (b). The average effective conductivity of the gold-sputtered plates is 1.6×10^7 S/m and loss per unit length is 1.1 dB/cm. The array achieves a realized gain of 29.5 dB at 350 GHz and 44.6 GHz of 3-dB gain bandwidth, while the impedance bandwidth ($|S_{11}| < -10$ dB) is 7.57% within a range of 338.2 to 364.7 GHz.

C. LENS ANTENNAS OR TRANSMIT-ARRAYS

Lens antenna absorbs many optical information engineering techniques and are used in a wider range of applications in communications and military. According to the theory of

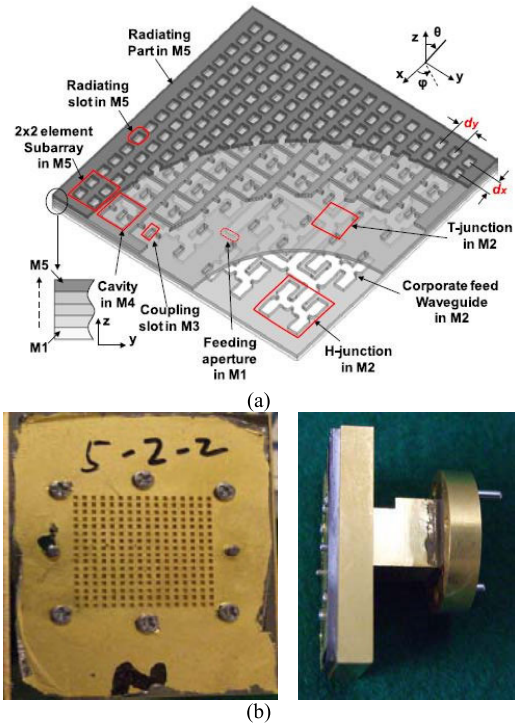

FIGURE 4. Waveguide slot antenna array in [54]: (a) Configuration of 16 × 16 slotted waveguide array (b) Top view and lateral view of fabricated array.

geometric optics, a spherical wave, which is radiated from a point source at the focal point of the lens, will condense through the lens to form a plane wave. This is the general idea of lens antenna design. During the transmission process, refraction occurs when waves pass through different media that are not parallel. The lens, which are mounted in front of the radiator, can concentrate the radiation energy and narrow the beam.

The authors in [57] present four different dielectric lens operating at V-band and H-band. Fig. 5 presents the lens fabricated by polymer-jetting 3-D printing technology. The 3-D printer has a fundamental resolution of 42 μm×42 μm×28 μm in x-, y-, and z-axes, respectively. The antenna fixture and lens are printed together, which can avoid assembly alignment errors. The fabricated V-band antennas are shown in Fig. 5 (a), the measured peak gain is ranging from 19.4 to 23.5 dBi (50-70 GHz). The measured beam directions at 50, 55, 60, 65, and 70 GHz. are −34°, −29°, −24.8°, −22°, and −19°, respectively. The fabricated H-band lens are shown in Fig. 5 (b), due to the uncertainties in dielectric property and loss of open-ended waveguide (OEW), the measured gain shifts downward by about 20 GHz and suffers from a 2-dB drop compared to the simulated results. The measured beam directions at 225, 250, 275, 300, and 325 GHz are −33.3°, −28.5°, −24.8°, −22°, and −19°, respectively.

Recently, the same research group in city university of Hong Kong designed another 3-D printed circularly polarized (CP) lens at H-band in [58]. Fig. 6 shows the lens fabricated

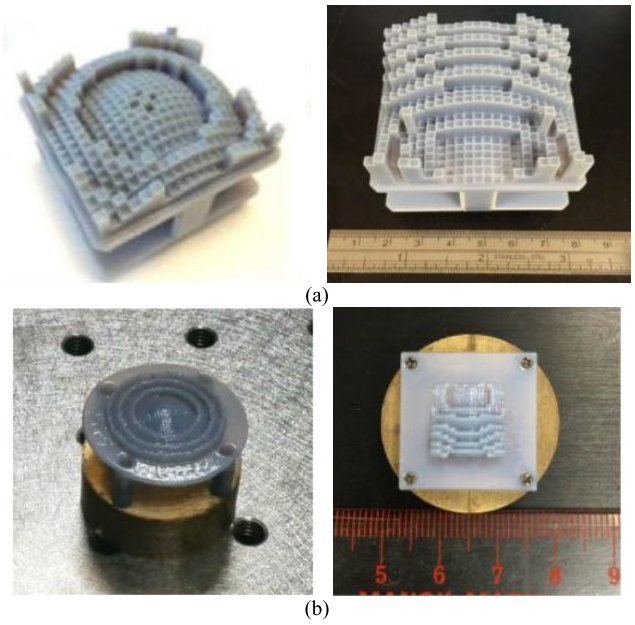

FIGURE 5. Fabricated lens antennas in [57]: (a) Lens antennas at V-band: left picture with fixed beam, right picture with scanning beam; (b) Lens antennas at H-band: left picture with fixed beam, right picture with scanning beam.

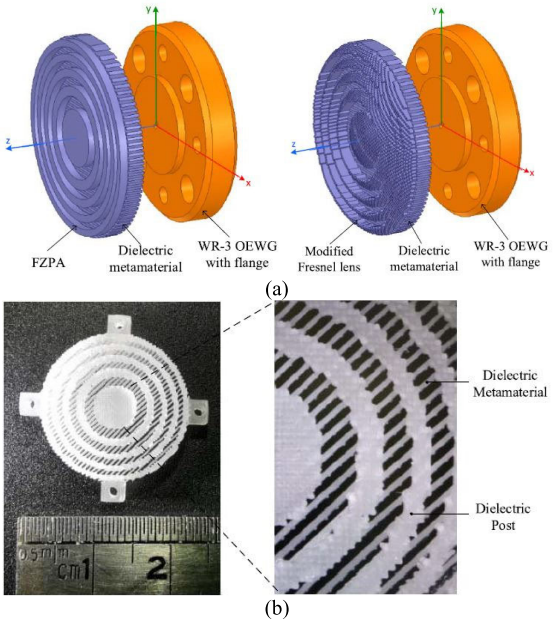

FIGURE 6. Lens antenna in [58]. (a) Designed 3-D models; (b) Fabricated lens antenna.

by in-house developed 3-D printing method with rapid prototyping technology. Considering the transmission phase of the dielectric post is sensitive to its height and the 3-D printer provides the highest resolution of 25 μm along the z-axis. The reflection coefficients of the designed antenna are smaller than −13.0 dB ranging from 265 to 320 GHz. The average gain of this CP lens is around 25 dBic, and the peak gain reaches to 27.4 dBic at 300 GHz, corresponding an aperture

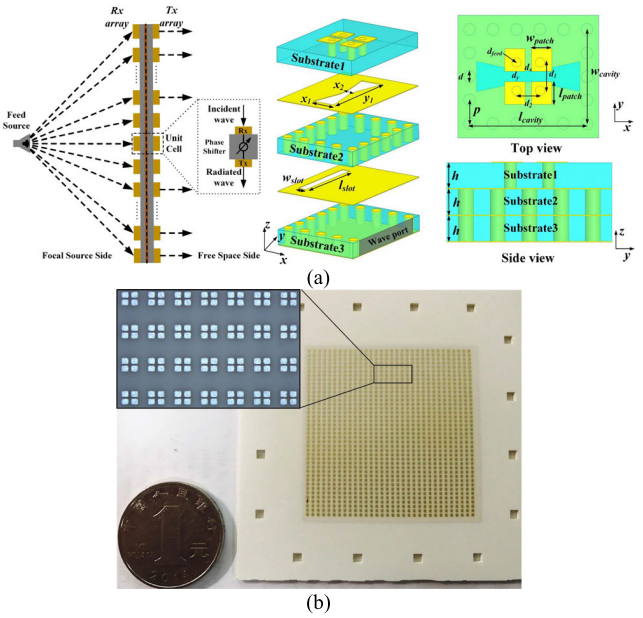

FIGURE 7. Wideband transmit-array in [59]. (a) Operation principle of a TA antenna and the designed radiation element; (b) Fabricated TA antenna.

efficiency of 15.4%. The measured 3-dB gain bandwidth is larger than 15.1% (275–320 GHz), and the 3 dB axial ratio (AR) bandwidth is larger than 18.8% (265–320 GHz).

Transmit-arrays (TA) schematized in Fig. 7 (a), which consist of an array of transmitting elements with independent phase adjustability, are one of the most attractive research areas in high-gain antennas due to the favorable features such as high gain, high aperture efficiency, low profile, and easy fabrication. Fig. 7 shows such a design reported at D-band in [59]. As shown in Fig. 7 (a), the proposed unit cell is composed of a pair of wideband magneto-electric dipoles, together with a substrate-integrated waveguide (SIW) aperture-coupling transmission structure for independent phase adjustability. This element provides a full 360° phase coverage and realizes nearly parallel phase response in a wide frequency range. A 40 × 32 array is fabricated by LTCC technology. The measured peak gain of the TA prototype is 33.45 dBi at 150 GHz with the aperture efficiency of 44.03%, and the measured 3-dB gain bandwidth is 124–158 GHz (24.29%).

D. REFLECT-ARRAYS

As with the principle of TA, reflect-arrays (RA) combine the advantages of reflector and array antennas. A dielectric reflectarray working at 220 GHz is reported in [64]. As shown in Fig. 8 (a), the reflectarray unit cell consists of a ground plane and a dielectric block. The reflection phase is obtained by adjusting the height of the block. Using the reflection phase computational algorithm, a dielectric reflectarray composed by 40 × 40 unit cells is designed and fabricated through 3DP technology. The maximum gain of 31.3 dBi and an aperture efficiency of 27.6% are obtained, and the 1-dB gain bandwidth is about 20.9% (220–246 GHz).

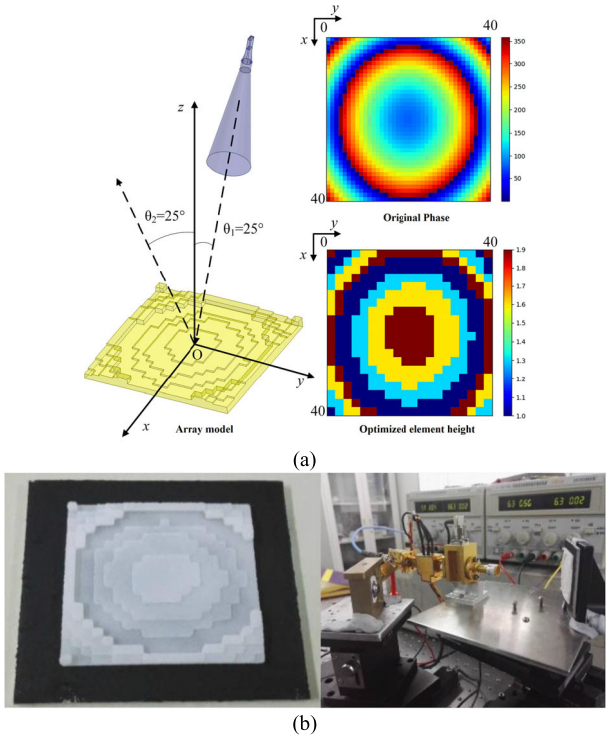

FIGURE 8. Wideband RA in [64]. (a) Designed dielectric reflectarray; (b) Fabricated RA antenna and the test enviroment.

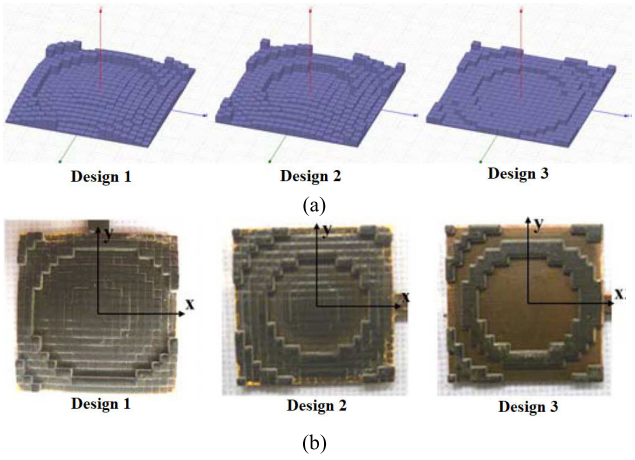

FIGURE 9. Three 3DP RAs in [65]. (a) Designed 3-D models; (b) Fabricated RA antennas.

The authors in [65] present another three different dielectric RAs operating at 100 GHz. Fig. 9 (b) presents the reflectarrays fabricated by Objet Eden 350 polymer-jetting rapid prototyping 3-D printer. The material loss and dielectric constant at 100 – 600 GHz are first observed using THz time-domain spectrometer system. Then RAs with different aperture phase distributions are studied to quantify the fabrication limits. The measured gain of the three prototypes at 100 GHz is 22.5, 22.9, and 18.9 dB, respectively. The proposed methodology is readily scalable and with the current material and fabrication technology, low-cost, high-gain antennas up to 1.0 THz can be realized.

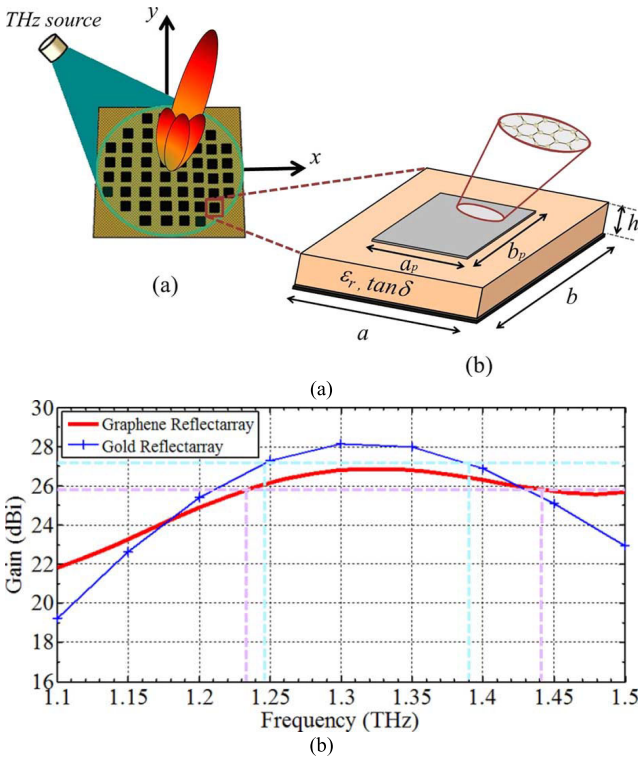

FIGURE 10. Wideband RA in [66]. (a) Designed dielectric reflectarray; (b) Fabricated RA antenna and the test enviroment.

With the rapid development of graphene preparation technology, graphene materials are also popular in THz high-gain antenna design. The work in [66] evaluates the feasibility of a fixed beam RA at THz band based on graphene and compares its performance to a similar implementation using gold for the first time. The designed graphene antenna operates at 1.3 THz and comprises 25448 electrically small unit cells. As shown in Fig. 10 (b), compared to a gold patches implementation, it exhibits better bandwidth and easier design thanks to the low sensitivity of the elements to the angle of incidence, but at the cost of increased loss. A 1-dB-gain bandwidth of 15% and 11% is achieved for graphene and gold RAs, respectively. The graph also reveals the lower maximum gain of the array made with graphene, which is due to the higher ohmic loss in graphene than gold at such frequencies. Since graphene complex conductivity can be efficiently controlled via electric-field biasing, RAs based on this material could potentially be dynamically reconfigured in the near future.

E. RESONANT CAVITY ANTENNAS

Resonant cavity antennas (RCAs) are excellent candidates to form planar structure, low loss, and high gain. RCA is constituted by suspending a partially reflective surface (PRS) above a ground plane at a predetermined height. There are many RCAs that work at X-band and Ka-band [71]–[77], but few works at the V-band [78]–[82], let alone the antennas that operate at THz band.

A novel wideband and high-gain RCA is presented in [78], which is achieved by FPC and printed ridge-gap waveguide

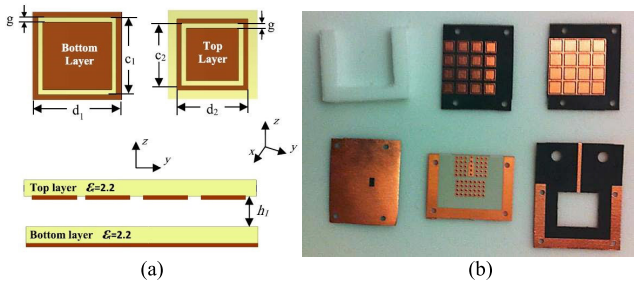

FIGURE 11. Fabry–Perot cavity in [78]. (a) Unit cell of the bottom and top layers of the PRS; (b) Fabricated prototype of the FPC antenna.

technologies. This work is the first one to utilize a PRS superstrate at 60 GHz to enhance the radiation characteristics. The FPC is formed by placing a dual-layer PRS above a slot antenna operating at 60 GHz, and fed by a printed ridge-gap waveguide. The structure of PRS is shown in Fig. 11 (a), it is a 2-D printed unit cell, and the unit cell is composed by two different frequency-selective surfaces (FSS) provides. This antenna is fabricated by PCB technology. The impedance bandwidth of the proposed antenna is 18.4%, (55.4-66.6 GHz). The maximum gain of 16.8 dBi is achieved.

Recently, the research group in city university of Hong Kong reported two RCAs operating at 60 GHz. This work introduces a new structure of PRS to realize gain enhancement. It is the first attempt to apply a fresnel zone plate (FZP) to a single-layer PRS. As shown in Fig. 12 (a), this antenna uses a substrate-integrated quasi-curve reflector and a FZP integrated PRS to form a FPC. With the quasi-curve reflector, multiple resonate modes are excited, providing a wide 3-dB gain bandwidth. This antenna is processed by low-cost and mature PCB technology. The antenna illustrates 17.8% impedance bandwidth from 54 to 64.5 GHz, and the 3-dB gain bandwidth is about 13.3 % (56-64 GHz). The measured peak gain is 21.0 dBi at broadside direction.

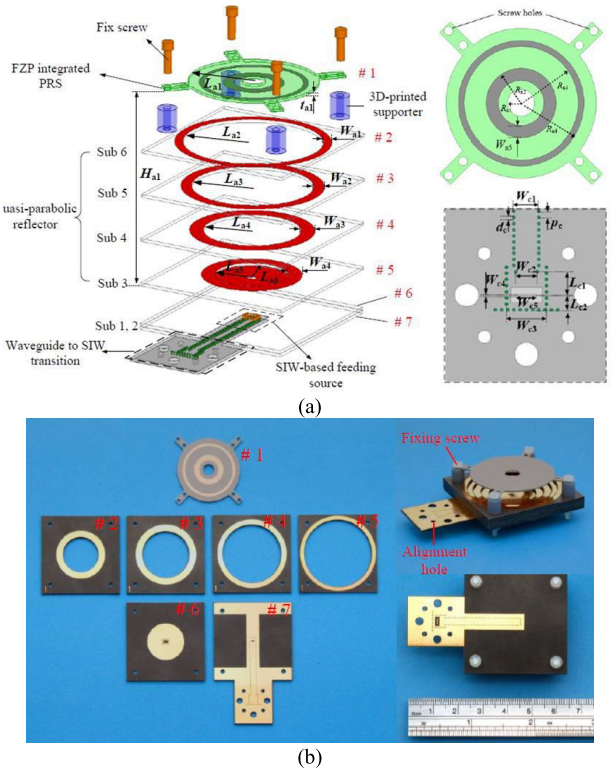

FIGURE 12. Fabry–Perot cavity in [79]. (a) Unit cell of the bottom and top layers of the PRS; (b) Fabricated prototype of the FPC antenna.

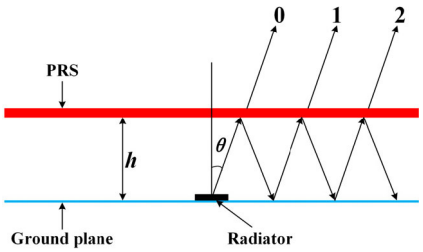

FIGURE 13. Schematic model of FPC PRS antenna.

III. CASE STUDY: BROADBAND AND HIGH-GAIN FPC ANTENNAS FOR LOW-TERAHERTZ APPLICATION

A. RCA PRINCIPLE

Ray-tracing analysis explains the requirement for broadband performance of FPC [84]. As shown in Fig. 13, in order to produce high directivity within a range of frequencies, the resonant condition of the cavity should be satisfied within this range. Maximum boresight gain is obtained at resonant frequency f_r when

$$h = \frac{c}{4\pi f_r}\left[\phi_{PRS} + (2N-1)\pi\right], \quad N=0,1,2.\ldots. \tag{1}$$

where ϕ_{PRS} is the phase of the PRS reflection coefficient, h is distance between PRS and ground. The resonant distance h is a function of the resonance frequency and the reflection coefficient of the PRS. The gain and bandwidth of the resonant structure can be increased by optimizing the reflection characteristics (magnitude and phase) of PRS.

To obtain maximum gain within a frequency range, the phase of reflection coefficient of the PRS should satisfy the following equation:

$$\phi_{PRS} = \frac{4\pi h}{c} f_r - (2N-1)\pi, \quad N=0,1,2.\ldots. \tag{2}$$

Actually, the directivity of FPCA includes two sections, one is the directivity of feed antenna and the other is the directivity of PRS, which can be expressed as in (3).

$$D = D_{feed} + D_{PRS} \tag{3}$$

where D_{feed} is the directivity of feed antenna, and D_{PRS} can be calculated by formula (4),

$$D_{PRS} = 10\log\frac{1+R}{1-R} \tag{4}$$

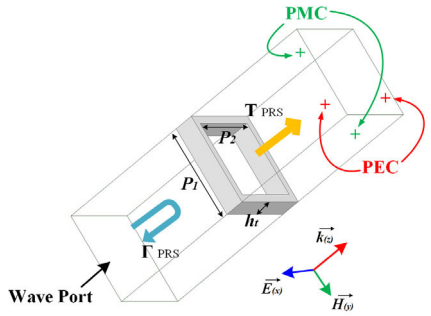

FIGURE 14. Unit cell of PRS.

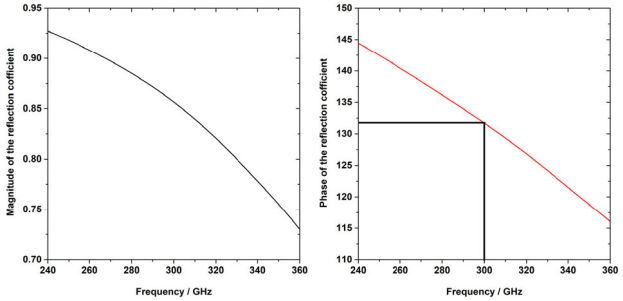

FIGURE 15. Simulated (a) magnitude (b) phase of the reflection coefficient.

B. ANTENNA DESIGN

Periodic metallic grid FSS is an ideal candidate PRS which can exhibit high reflectivity at the desired frequency. Fig.14 shows the designed PRS unit cell with geometrical parameters. Periodicity of the unit cell P_1 is 0.48 mm. The inner dimension and thickness are $P_2 = 0.4$ and $h_t = 0.1$ mm, respectively. The size of P_1 and P_2 is close to half wavelength at 300 GHz. In order to ensure the realization of processing, the width of square ring is 0.1 mm. The equivalent model of the periodic structure of the square ring is a high pass filter. From the frequency characteristics, it will reflect the low-frequency wave and transmit the high-frequency wave. High Frequency Structure Simulator (HFSS) is used to optimize the parameters of unit cell. The simulated magnitude and phase of the reflection coefficient are shown in Fig. 15. From the simulated result, the phase of PRS at 300 GHz is 132°, the distance between the feed antenna and the PRS layer h could be calculated by (1).

$$h = \frac{c}{4\pi f_r}[\phi_{PRS} + (2N-1)\pi] = \frac{300/300}{2}(\frac{132}{2\pi} + 0.5) \approx 0.433(mm) \quad (1)$$

The exploded view of the complete FPC antenna is shown in Fig. 16, which is composed of a WR3 waveguide feed port, a coupling slot, transmission cavity, two radiating slots and 5×5 metal PRS superstate. The metal wall is used to support the PRS layer on the top of radiating slots. Direct illumination

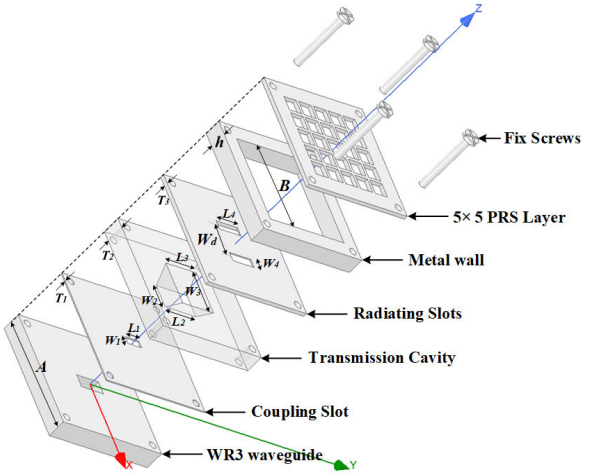

FIGURE 16. The exploded view of the proposed antenna $W_1 = 0.2$, $L_1 = 0.44$, $W_2 = 1.0$, $L_2 = 0.63$, $W_3 = 1.2$, $L_3 = 0.63$, $W_4 = 0.25$, $L_2 = 0.7$, $W_d = 0.95$, $T_1 = 0.03$, $T_2 = 0.55$, $T_3 = 0.03$, $A = 3.2$, $B = 2.4$, $h = 0.44$, unit: mm.

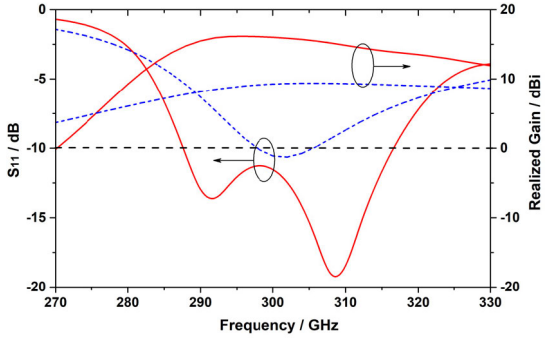

FIGURE 17. Simulated S_{11} and antenna gain with and without PRS.

of the PRS will lead to impedance mismatching, then to decrease the antenna efficiency. Therefore, a novel transition structure is used to realize impedance matching. A small slot is excited by the WR3 waveguide port. The middle layer adopts a trapezoidal cavity to transmit the wave from the coupling slot. On the top of the trapezoidal cavity, two identical, symmetrical parallel radiating slots are used to broaden the impedance matching bandwidth. Simulated return loss and gain of antenna with and without PRS are shown in Fig. 17. It can be seen that both the impedance matching performance and the realized gain are well improved. The antenna achieves a peak of 16.2 dBi at 295 GHz. As shown in Fig. 17, this transition layer will generate additional modes at the frequencies of 290 and 310 GHz, respectively.

Fig. 18 gives the E-field distributions and 3D radiation patterns of antenna with and without PRS at 300 GHz. Due to the large distance between two radiating slots, the antenna without PRS presents another two large electric fields at the low elevation angle. After add the 5×5 metal PRS superstate, the EM energy converges along the boresight direction.

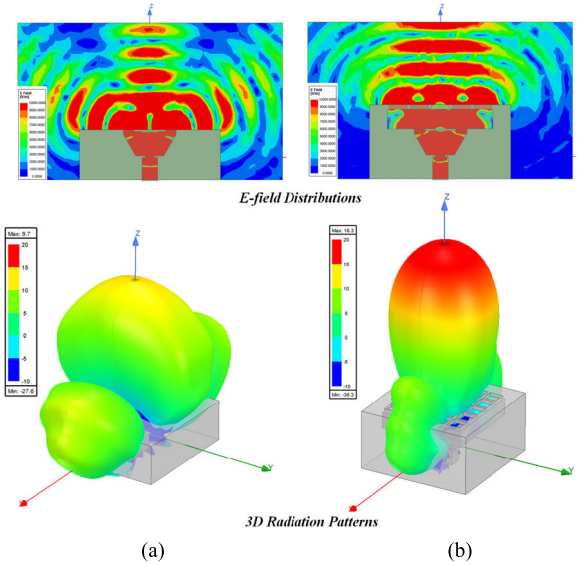

FIGURE 18. Simulated E-field distributions and 3D radiation patterns of antenna (a) without PRS, (b) with PRS.

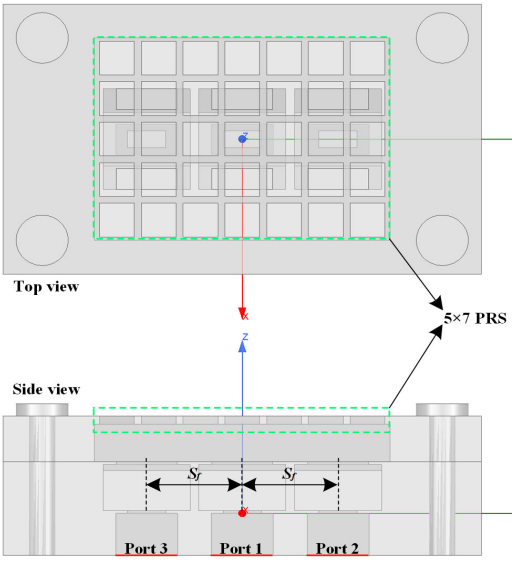

FIGURE 19. Configuration of proposed multibeam FPC antenna.

In addition, this antenna prototype is suitable for multi-beam applications. As shown in Fig. 19, a three-switched-beam FPC is designed by three feeding sources to realize switched-beam function. All the dimensions are the same as the antenna element as shown in Fig. 16. The offset distance between these three feeding sources (Port 1, 2, and 3), which are symmetrically placed, is $S_f = 1.1$ mm. When the feeding source is placed at a distance from y-axis ($S_f \neq 0$ mm), the phase distribution of the PRS will be changed. The simulated S-parameters of these three feeding ports is illustrated in Fig. 20. An overlapped impedance bandwidth from 290 to 320 GHz is achieved. When one port is excited, the other two ports are matched. As a result, the radiation pattern is tilted as shown in Fig. 21.

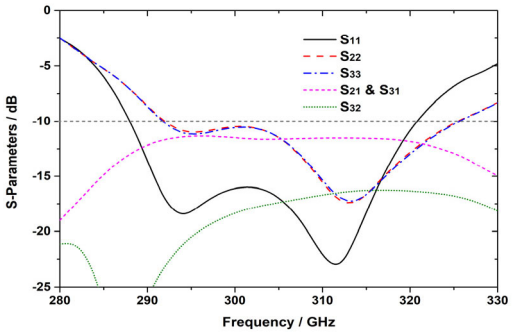

FIGURE 20. Simulated S-Parameters of multibeam FPC antenna.

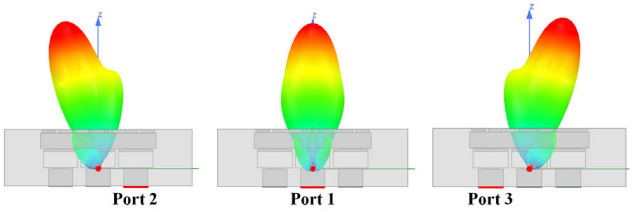

FIGURE 21. Tilted Radiation patterns with different feeding ports.

Fig. 22 shows the simulated radiation patterns at different frequencies (290, 300, and 310 GHz) with three beams. As shown in Fig. 21 (a), the peak realized gain at 290 GHz is 15.37 dBi with normal patterns and the peak gain of tilted patterns is 13.6 dBi with $\theta = 8°$. While, when the frequency increases to 300 GHz, the boresight peak gain becomes 15.47 dBi, and the tilted patterns peak gain, which is 16.29 dBi, occurs at $\theta = 14°$. As shown in Fig. 21 (c), as the frequency increases further, the phase change of PRS is more dramatical, which leads to the deterioration of normal patterns at 310 GHz, and the peak gain decreases to 12.20 dBi. However, the peak gain of tilted patterns is 15.54 dBi at $\theta = 18°$.

C. FABRICATION AND MEASUREMENT

For 300 GHz FPC antenna design, almost none of the available AM or 3D techniques are capable of printing such fine structures. Therefore, this session mainly focus on the printing of scaled element at 30GHz. Based on the 300 GHz design, a scaled model operating at 30 GHz is simulated. As the whole antenna is made of metal, the values of antenna parameters are ten times than those at 300 GHz given in Fig. 16. The feeding rectangular waveguide adopts WR-28 with recommended frequency band of operation from 26.5 to 40 GHz.

There is a variety of AM processes. Here we use Metal Binder Jetting (MBJ), which is the most commonly used method for printing metallic structure. The 3D printer is ProX DMP 100 as shown in Fig. 23 (a). It is a high quality direct metal printing (DMP) system. During the fabrication, loose metal powder particles are melted together by

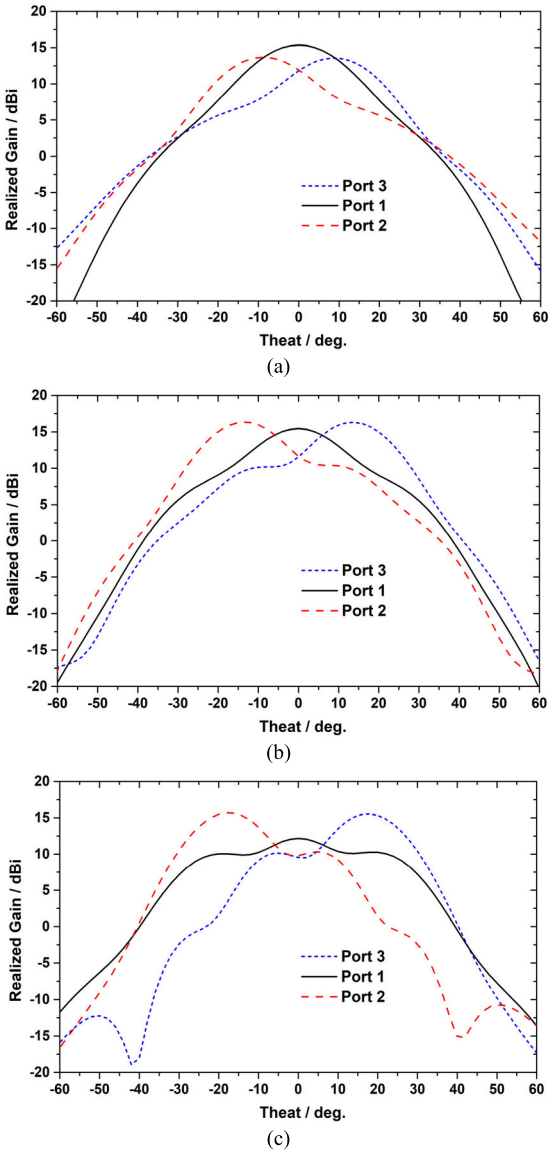

FIGURE 22. Radiation patterns of the proposed multibeam FPC antenna at (a) 290, (b) 300, and (c) 310 GHz.

a high-precision laser. The laser is directed to the powder particles according to the STL file of the antenna structure in order to selectively build up thin subsequent horizontal layers. Bonding the layers together forms the final metal parts as shown in Fig. 23 (b). MBJ process can create complicated and highly detailed design in a very short period. Moreover, it is cost-effective compared with traditional manufacturing technique.

This antenna is measured in an anechoic chamber using Anritsu 37397C VNA. Reasonable agreement between the measured and the simulated return loss is achieved, which is shown in Fig. 24. The difference mainly attributes to the surface roughness and tolerance during the fabrication process. The accuracy of the attachment of the waveguide-coax adapter to the WR-28 waveguide feed is another key factor with respect to the measured return loss.

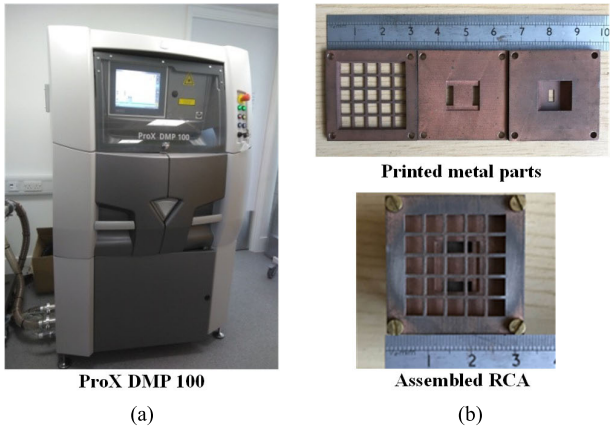

FIGURE 23. The printer and printed antenna.

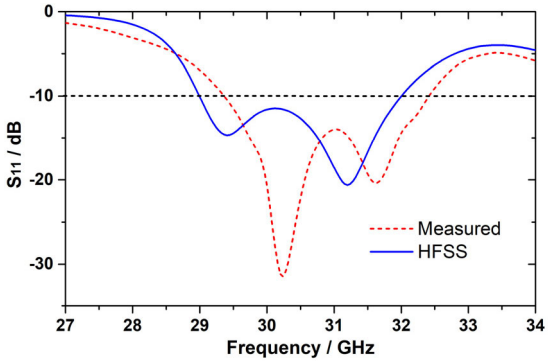

FIGURE 24. Simulated and measured S_{11}.

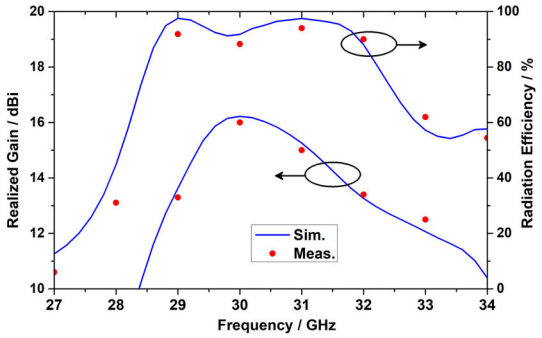

FIGURE 25. Simulated and measured antenna gain and radiation efficiency.

Fig. 25 compares the simulated and measured results of antenna realized gain and radiation efficiency. We can get the conclusion that the fabricated 3DP antenna has a good radiation performance. Compared with the simulated result, the measured result is slightly smaller from 28 to 31 GHz and higher from 32 to 33 GHz. A 3-dB-gain bandwidth of 10% is achieved. Both the simulated and measured antenna radiation efficiency are more than 88%. The small discrepancy attributes to the fabrication and assembly tolerances.

TABLE 1. Comparison among different Low-THz high gain antennas.

Ref.	Antenna Type	Antenna Size (mm)	Antenna Working Band	Fabrication Technique	Structural Complexity	Cost	3 dB Gain Bandwidth / %	Peak Gain / dB
[50]	Horn	Φ=21.34	D-band	3DP (All metal)	Easy	Low	42.4	24.5
[51]		2.8×3.2	H-band	PCB & LTCC (Dielectric and metal layers)	Hard	High	24	18
[52-53]	Planar waveguide array	67.2×67.2 (32×32 array)	D-band	Diffusion Bonding (All metal)	Hard	High	11.9	39.1
[54]		11×11	H-band	Silicon & Diffusion Bonding (All metal)	complex	High	11.8	30.6
[57]	Lens	5.25×5.25	H-band	3DP (Dielectric layers)	Easy	Low	21.7	27
[58]		Φ=20	H-band	3DP (Dielectric layers)	Easy	Low	15.1	27.4 (CP)
[59]	Transmit-array	40×40	D-band	PCB & LTCC (Dielectric and metal layers)	Hard	High	24.4	33.45
[64]	Reflect-array	28×28	H-band	3DP (Dielectric layers)	Easy	Low	–	27.4
[65]		30×30	W-band	3DP (Dielectric layers)	Easy	Low	–	22.5
[66]		Φ=2.52	1.3 THz	Graphene	Easy	High	–	27
[71]	RCA	12×12	V-band	PCB (Dielectric and metal layers)	Hard	Low	12.5	16.8
[72]		Φ=39.6	V-band	PCB (Dielectric and metal layers)	complex	Low	13.3	21
This Work		2.4×2.4 (Simulated)	H-band	3DP	Simple	--	9.9	16.2
		24×24 (Fabricated)	Ka-band	3DP (All metal)	Simple	Low	10	16

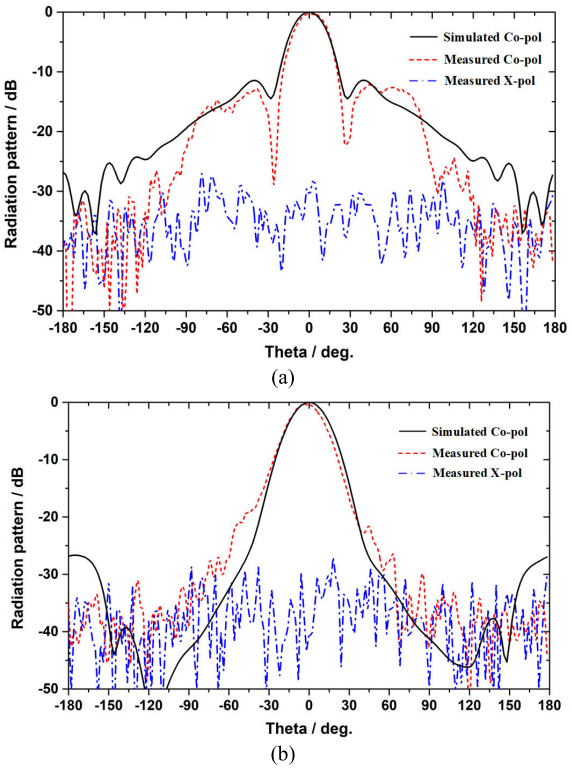

FIGURE 26. Simulated and measured normalized radiation patterns at 30 GHz. (a) E-plane, and (b) H-plane.

The normalized measured radiation patterns at 30 GHz in both E and H planes are shown in Fig. 26. The cross-polarization level is well suppressed, which is no greater than −30 dB in both planes. Sidelobe levels (SLLs) in E and H planes are less than −10 dB and −20 dB, respectively. Although the asymmetric fabricated structure causes slight asymmetry in the sidelobes, the main lobes keep good performances, agreeing well with the simulated results. The 3-dB beamwidth of both planes is in good agreement with simulated results.

IV. CONCLUSION AND FURURE WORK

For Low-THz band, fabrication accuracy is crucial with respect to antenna performance. Traditional fabrication methods of THz devices can be an expensive and time-consuming effort. This paper reviews the current state of the art of wideband Low-THz antennas with corresponding manufacturing processes and different techniques used by researchers for gain enhancement. Then a novel FPC antenna element and three-switched-beam antenna are designed at 300 GHz. To validate the high-performance of proposed antenna, a scaled antenna element working at 30 GHz is fabricated using MBJ process, which is fast and cost-effective compared with traditional manufacturing technique. Reasonable agreements are achieved between simulated and measured results. Table 1 gives a comparison among different high gain antenna

in Low-THz band. A detailed comparison from antenna type, antenna size, working frequency band, processing method, and radiation performance is illustrated in Table 1. The results show that our antenna is currently the first one antenna, which is achieved with very simple all metal RCA structure in millimeter-wave & Low-THz band using viable AM techniques to realize high gain and multi-beam radiation. The measured results proved that manufacturing parts have a high resolution. With the improvements of AM precision, some new printing technologies could be used to fabricate our Low-Thz antennas in the near future, such as hybrid 3DP and 4D printing technology. The next step, our aim is to design and fabricate a Low-THz active phased array system, which will integrate some active circuits (oscillators, amplifiers) and passive circuits (filters) into one single chip. In addition, we will do some researches on Low-Thz frequency scanning antennas.

REFERENCES

[1] P. H. Siegel, "Terahertz technology," *IEEE Trans. Microw. Theory Techn.*, vol. 50, no. 3, pp. 910–928, Mar. 2002.
[2] H.-J. Song and T. Nagatsuma, "Present and future of terahertz communications," *IEEE Trans. THz Sci. Technol.*, vol. 1, no. 1, pp. 256–263, Sep. 2011.
[3] R. Piesiewicz, T. Kleine-Ostmann, N. Krumbholz, D. Mittleman, M. Koch, J. Schoebei, and T. Kurner, "Short-range ultra-broadband terahertz communications: Concepts and perspectives," *IEEE Antennas Propag. Mag.*, vol. 49, no. 6, pp. 24–39, Dec. 2007.
[4] G. P. Williams, "Filling the THz gap—High power sources and applications," *Rep. Progr. Phys.*, vol. 69, no. 2, pp. 301–326, Feb. 2006.
[5] S. A. Kuznetsov, M. Navarro-Cía, V. V. Kubarev, A. V. Gelfand, M. Beruete, I. Campillo, and M. Sorolla, "Regular and anomalous extraordinary optical transmission at the THz-gap," *Opt. Express*, vol. 17, no. 14, pp. 11730–11738, Jul. 2009.
[6] F. Norouzian, E. Marchetti, M. Gashinova, E. Hoare, C. Constantinou, P. Gardner, and M. Cherniakov, "Rain attenuation at millimeter wave and low-THz frequencies," *IEEE Trans. Antennas Propag.*, vol. 68, no. 1, pp. 421–431, Jan. 2020.
[7] F. Norouzian, R. Du, E. G. Hoare, P. Gardner, C. Constantinou, M. Cherniakov, and M. Gashinova, "Low-THz transmission through water-containing contaminants on antenna radome," *IEEE Trans. THz Sci. Technol.*, vol. 8, no. 1, pp. 63–75, Jan. 2018.
[8] W. Ning, F. Qi, Z. Liu, Y. Wang, H. Wu, and J. Wang, "Resolution enhancement in terahertz imaging via deconvolution," *IEEE Access*, vol. 7, pp. 65116–65121, 2019.
[9] K. B. Cooper and R. J. Dengler, "A high-resolution imaging radar at 580 GHz," *IEEE Trans. Microw. Wireless Compon. Lett.*, vol. 18, no. 1, pp. 64–66, Jan. 2008.
[10] C. Ciano, M. Flammini, V. Giliberti, P. Calvani, E. DelRe, F. Talarico, M. Torre, M. Missori, and M. Ortolani, "Confocal imaging at 0.3 THz with depth resolution of a painted wood artwork for the identification of buried thin metal foils," *IEEE Trans. THz Sci. Technol.*, vol. 8, no. 4, pp. 390–396, Jul. 2018.
[11] A. Mostajeran, S. M. Naghavi, M. Emadi, S. Samala, B. P. Ginsburg, M. Aseeri, and E. Afshari, "A high-resolution 220-GHz ultra-wideband fully integrated ISAR imaging system," *IEEE Trans. Microw. Theory Techn.*, vol. 67, no. 1, pp. 429–442, Jan. 2019.
[12] Z. D. Taylor, R. S. Singh, D. B. Bennett, P. Tewari, C. P. Kealey, N. Bajwa, M. O. Culjat, A. Stojadinovic, H. Lee, J.-P. Hubschman, E. R. Brown, and W. S. Grundfest, "THz medical imaging: *In vivo* hydration sensing," *IEEE Trans. THz Sci. Technol.*, vol. 1, no. 1, pp. 201–219, Sep. 2011.
[13] Y. C. Sim, K.-M. Ahn, J. Y. Park, C.-S. Park, and J.-H. Son, "Temperature-dependent terahertz imaging of excised oral malignant melanoma," *IEEE Biomed. Health Infor.*, vol. 17, no. 4, pp. 779–784, Jul. 2013.
[14] Y. C. Sim, K.-M. Ahn, J. Y. Park, C.-S. Park, and J.-H. Son, "Temperature-dependent terahertz imaging of excised oral malignant melanoma," *IEEE Trans. THz Sci. Technol.*, vol. 3, no. 4, pp. 368–373, Jul. 2013.
[15] A. Afsharinejad, A. Davy, B. Jennings, and C. Brennan, "Performance analysis of plant monitoring nanosensor networks at THz frequencies," *IEEE Internet Things J.*, vol. 3, no. 1, pp. 59–69, Feb. 2016.
[16] P. Thoma, A. Scheuring, S. Wunsch, K. Il'in, A. Semenov, H.-W. Hubers, V. Judin, A.-S. Muller, N. Smale, M. Adachi, S. Tanaka, S.-I. Kimura, M. Katoh, N. Yamamoto, M. Hosaka, E. Roussel, C. Szwaj, S. Bielawski, and M. Siegel, "High-speed Y–Ba–Cu–O direct detection system for monitoring picosecond THz pulses," *IEEE Trans. THz Sci. Technol.*, vol. 3, no. 1, pp. 81–86, Jan. 2013.
[17] J. Zdanevicius, H.-W. Hubers, H. G. Roskos, D. Cibiraite, K. Ikamas, M. Bauer, J. Matukas, A. Lisauskas, H. Richter, T. Hagelschuer, and V. Krozer, "Field-effect transistor based detectors for power monitoring of THz quantum cascade lasers," *IEEE Trans. Terahertz Sci. Technol.*, vol. 8, no. 6, pp. 613–621, Nov. 2018.
[18] J. Grzyb, K. Statnikov, N. Sarmah, B. Heinemann, and U. R. Pfeiffer, "A 210–270-GHz circularly polarized FMCW radar with a single-lens-coupled SiGe HBT chip," *IEEE Trans. THz Sci. Technol.*, vol. 6, no. 6, pp. 771–783, Nov. 2016.
[19] L. Daniel, A. Stove, E. Hoare, D. Phippen, M. Cherniakov, B. Mulgrew, and M. Gashinova, "Application of Doppler beam sharpening for azimuth refinement in prospective low-THz automotive radars," *IET Radar, Sonar Navigat.*, vol. 12, no. 10, pp. 1121–1130, Oct. 2018.
[20] S. Gui, J. Li, and Y. Pi, "Security imaging for multi-target screening based on adaptive scene segmentation with terahertz radar," *IEEE Sensors J.*, vol. 19, no. 7, pp. 2675–2684, Apr. 2019.
[21] R. Knipper, A. Brahm, E. Heinz, T. May, G. Notni, H.-G. Meyer, A. Tunnermann, and J. Popp, "THz absorption in fabric and its impact on body scanning for security application," *IEEE Trans. THz Sci. Technol.*, vol. 5, no. 6, pp. 999–1004, Nov. 2015.
[22] R. Appleby and R. N. Anderton, "Millimeter-wave and submillimeter-wave imaging for security and surveillance," *Proc. IEEE*, vol. 95, no. 8, pp. 1683–1690, Aug. 2007.
[23] Z. Wang, M. Hu, E. E. Kuruoglu, W. Zhu, and G. Zhai, "How do detected objects affect the noise distribution of terahertz security images?" *IEEE Access*, vol. 6, pp. 41087–41092, 2018.
[24] R. Zhang, J. Zhou, J. Lan, B. Yang, and Z. Yu, "A high-precision hybrid analog and digital beamforming transceiver system for 5G millimeter-wave communication," *IEEE Access*, vol. 7, pp. 83012–83023, 2019.
[25] Q. Wu, J. Hirokawa, J. Yin, C. Yu, H. Wang, and W. Hong, "Millimeter-wave multibeam endfire dual-circularly polarized antenna array for 5G wireless applications," *IEEE Trans. Antennas Propag.*, vol. 66, no. 9, pp. 4930–4935, Sep. 2018.
[26] M. Imbert, J. Romeu, M. Baquero-Escudero, M.-T. Martinez-Ingles, J.-M. Molina-Garcia-Pardo, and L. Jofre, "Assessment of LTCC-based dielectric flat lens antennas and switched-beam arrays for future 5G millimeter-wave communication systems," *IEEE Trans. Antennas Propag.*, vol. 65, no. 12, pp. 6453–6473, Dec. 2017.
[27] T. S. Rappaport, G. R. MacCartney, M. K. Samimi, and S. Sun, "Wideband millimeter-wave propagation measurements and channel models for future wireless communication system design," *IEEE Trans. Commun.*, vol. 63, no. 9, pp. 3029–3056, Sep. 2015.
[28] M. Katz, P. Pirinen, and H. Posti, "Towards 6G: Getting ready for the next decade," in *Proc. 16th Int. Symp. Wireless Commun. Syst. (ISWCS)*, Aug. 2019, pp. 714–718.
[29] P. T. Dat, A. Kanno, K. Inagaki, T. Umezawa, N. Yamamoto, and T. Kawanishi, "Hybrid optical wireless-mmWave: Ultra high-speed indoor communications for beyond 5G," in *Proc. IEEE Conf. Comput. Commun. Workshops*, Apr. 2019, pp. 1003–1004.
[30] M. Katz, M. Matinmikko-Blue, and M. Latva-Aho, "6Genesis flagship program: Building the bridges towards 6G-enabled wireless smart society and ecosystem," in *Proc. IEEE 10th Latin-Amer. Conf. Commun. (LATINCOM)*, Nov. 2018, pp. 1–9.
[31] X. Yang, Y. Pi, T. Liu, and H. Wang, "Three-dimensional imaging of space debris with space-based terahertz radar," *IEEE Sensors J.*, vol. 18, no. 3, pp. 1063–1072, Feb. 2018.
[32] M. C. Wiedner, I. Mehdi, A. Baryshev, V. Belitsky, V. Desmaris, A. M. DiGiorgio, J.-D. Gallego, M. Gerin, P. Goldsmith, F. Helmich, W. Jellema, A. Laurens, C. Risacher, A. Cooray, and M. Meixner, "A proposed heterodyne receiver for the origins space telescope," *IEEE Trans. THz Sci. Technol.*, vol. 8, no. 6, pp. 558–571, Oct. 2018.
[33] P. H. Siegel, "THz instruments for space," *IEEE Trans. Antennas Propag.*, vol. 55, no. 11, pp. 2957–2965, Nov. 2007.

[34] O. Mitrofanov, R. James, F. A. Fernandez, T. K. Mavrogordatos, and J. A. Harrington, "Reducing transmission losses in hollow THz waveguides," *IEEE Trans. THz Sci. Technol.*, vol. 1, no. 1, pp. 124–132, Sep. 2011.

[35] F. Fesharaki, T. Djerafi, M. Chaker, and K. Wu, "Low-loss and low-dispersion transmission line over DC-to-THz spectrum," *IEEE Trans. THz Sci. Technol.*, vol. 6, no. 4, pp. 611–618, Jul. 2016.

[36] A. Barh, R. K. Varshney, B. P. Pal, G. P. Agrawal, and B. M. A. Rahman, "Design of a polymer-based hollow-core bandgap fiber for low-loss terahertz transmission," *IEEE Photon. Technol. Lett.*, vol. 28, no. 15, pp. 1703–1706, Aug. 1, 2016.

[37] G. A. Komandin, S. V. Chuchupal, S. P. Lebedev, Y. G. Goncharov, A. F. Korolev, O. E. Porodinkov, I. E. Spektor, and A. A. Volkov, "BWO generators for terahertz dielectric measurements," *IEEE Trans. THz Sci. Technol.*, vol. 3, no. 4, pp. 440–444, Jul. 2013.

[38] S. Hisatake, J.-Y. Kim, K. Ajito, and T. Nagatsuma, "Self-heterodyne spectrometer using Uni-Traveling-Carrier photodiodes for terahertz-wave generators and optoelectronic mixers," *J. Lightw. Technol.*, vol. 32, no. 20, pp. 3683–3689, Oct. 15, 2014.

[39] J. Booske and R. Dobbs, "Vacuum electronic high power terahertz sources," *IEEE Trans. THz Sci. Technol.*, vol. 1, no. 1, pp. 54–75, Sep. 2011.

[40] S. Y. Jun, B. Sanz-Izquierdo, E. A. Parker, D. Bird, and A. McClelland, "Manufacturing considerations in the 3-D printing of fractal antennas," *IEEE Trans. Compon., Packag., Manuf. Technol.*, vol. 7, no. 11, pp. 1891–1898, Nov. 2017.

[41] S. Verploegh, M. Coffey, E. Grossman, and Z. Popovic, "Properties of 50–110-GHz waveguide components fabricated by metal additive manufacturing," *IEEE Trans. Microw. Theory Techn.*, vol. 65, no. 12, pp. 5144–5153, Dec. 2017.

[42] E. A. Rojas-Nastrucci, J. T. Nussbaum, N. B. Crane, and T. M. Weller, "Ka-band characterization of binder jetting for 3-D printing of metallic rectangular waveguide circuits and antennas," *IEEE Trans. Microw. Theory Techn.*, vol. 65, no. 9, pp. 3099–3108, Sep. 2017.

[43] R. Sorrentino and O. A. Peverini, "Additive manufacturing: A key enabling technology for next-generation microwave and millimeter-wave systems [point of view]," *Proc. IEEE*, vol. 104, no. 7, pp. 1362–1366, Jul. 2016.

[44] M. C. Lemme, T. J. Echtermeyer, M. Baus, and H. Kurz, "A graphene field-effect device," *IEEE Electron Device Lett.*, vol. 28, no. 4, pp. 282–284, Apr. 2007.

[45] W. Ernie Hill, "Graphene sensors," *IEEE Sensors J.*, vol. 11, no. 12, pp. 3161–3170, Dec. 2011.

[46] M. Esquius-Morote, J. S. Gomez-Diaz, and J. Perruisseau-Carrier, "Sinusoidally modulated graphene leaky-wave antenna for electronic beamscanning at THz," *IEEE Trans. THz Sci. Technol.*, vol. 4, no. 1, pp. 116–122, Jan. 2014.

[47] B. Sensale-Rodriguez, R. Yan, L. Liu, D. Jena, and H. G. Xing, "Graphene for reconfigurable terahertz optoelectronics," *Proc. IEEE*, vol. 101, no. 7, pp. 1705–1716, Jul. 2013.

[48] D. Correas-Serrano, J. S. Gomez-Diaz, J. Perruisseau-Carrier, and A. Álvarez-Melcón, "Graphene-based plasmonic tunable low-pass filters in the terahertz band," *IEEE Trans. Nanotechnol.*, vol. 13, no. 6, pp. 1145–1153, Nov. 2014.

[49] G. Oliveri, D. H. Werner, and A. Massa, "Reconfigurable electromagnetics through Metamaterials—A review," *Proc. IEEE*, vol. 103, no. 7, pp. 1034–1056, Jul. 2015.

[50] B. Zhang, Z. Zhan, Y. Cao, H. Gulan, P. Linner, J. Sun, T. Zwick, and H. Zirath, "Metallic 3-D printed antennas for Millimeter- and submillimeter wave applications," *IEEE Trans. THz Sci. Technol.*, vol. 6, no. 4, pp. 592–600, Jul. 2016.

[51] T. Tajima, H.-J. Song, K. Ajito, M. Yaita, and N. Kukutsu, "300-GHz step-profiled corrugated horn antennas integrated in LTCC," *IEEE Trans. Antennas Propag.*, vol. 62, no. 11, pp. 5437–5444, Nov. 2014.

[52] D. Kim, "4×4-element corporate-feed waveguide slot array antenna with cavities for the 120 GHz-band," *IEEE Trans. Antennas Propag.*, vol. 61, no. 12, pp. 5968–5975, Dec. 2013.

[53] D. Kim, J. Hirokawa, M. Ando, J. Takeuchi, and A. Hirata, "64×64-element and 32×32-element slot array antennas using double-layer hollow-waveguide corporate-feed in the 120 GHz band," *IEEE Trans. Antennas Propag.*, vol. 62, no. 3, pp. 1507–1512, Mar. 2014.

[54] K. Tekkouk, J. Hirokawa, K. Oogimoto, T. Nagatsuma, H. Seto, Y. Inoue, and M. Saito, "Corporate-feed slotted waveguide array antenna in the 350-GHz band by silicon process," *IEEE Trans. Antennas Propag.*, vol. 65, no. 1, pp. 217–225, Jan. 2017.

[55] M. M. Zhou and Y. J. Cheng, "D-band high-gain circular-polarized plate array antenna," *IEEE Trans. Antennas Propag.*, vol. 66, no. 3, pp. 1280–1287, Mar. 2018.

[56] J. Xu, Z. N. Chen, X. Qing, and W. Hong, "140-GHz TE_{20}-mode dielectric-loaded SIW Slot antenna array in LTCC," *IEEE Trans. Antennas Propag.*, vol. 61, no. 4, pp. 1784–1793, Apr. 2013.

[57] H. Yi, S.-W. Qu, K.-B. Ng, C. H. Chan, and X. Bai, "3-D printed millimeter-wave and terahertz lenses with fixed and frequency scanned beam," *IEEE Trans. Antennas Propag.*, vol. 64, no. 2, pp. 442–449, Feb. 2016.

[58] G.-B. Wu, Y.-S. Zeng, K. F. Chan, S.-W. Qu, and C. H. Chan, "3-D printed circularly polarized modified fresnel lens operating at terahertz frequencies," *IEEE Trans. Antennas Propag.*, vol. 67, no. 7, pp. 4429–4437, Jul. 2019.

[59] Z.-W. Miao, Z.-C. Hao, G. Q. Luo, L. Gao, J. Wang, X. Wang, and W. Hong, "140 GHz high-gain LTCC-integrated transmit-array antenna using a wideband SIW aperture-coupling phase delay structure," *IEEE Trans. Antennas Propag.*, vol. 66, no. 1, pp. 182–190, Jan. 2018.

[60] L. P. Kamburov, J. M. Rodriguez, J. R. Urumov, and H. D. Hristov, "Millimeter-wave conical fresnel zone lens of flat dielectric rings," *IEEE Trans. Antennas Propag.*, vol. 62, no. 4, pp. 2140–2148, Apr. 2014.

[61] K. X. Wang and H. Wong, "A wideband millimeter-wave circularly polarized antenna with 3-D printed polarizer," *IEEE Trans. Antennas Propag.*, vol. 65, no. 3, pp. 1038–1046, Mar. 2017.

[62] C. Fan, W. Yang, W. Che, S. He, and Q. Xue, "A wideband and low-profile discrete dielectric lens using 3-D printing technology," *IEEE Trans. Antennas Propag.*, vol. 66, no. 10, pp. 5160–5169, Oct. 2018.

[63] G. B. Wu, Y.-S. Zeng, K. F. Chan, S.-W. Qu, and C. H. Chan, "High-gain circularly polarized lens antenna for terahertz applications," *IEEE Antennas Wireless Propag. Lett.*, vol. 18, no. 5, pp. 921–925, May 2019.

[64] M. D. Wu, B. Li, Y. Zhou, D. L. Guo, Y. Liu, F. Wei, and X. Lv, "Design and measurement of a 220 GHz wideband 3-D printed dielectric reflectarray," *IEEE Antennas Wireless Propag. Lett.*, vol. 17, no. 11, pp. 2094–2098, Nov. 2018.

[65] P. Nayeri, M. Liang, R. A. Sabory-Garcia, M. Tuo, F. Yang, M. Gehm, H. Xin, and A. Z. Elsherbeni, "3D printed dielectric reflectarrays: Low-cost high-gain antennas at sub-millimeter waves," *IEEE Trans. Antennas Propag.*, vol. 62, no. 4, pp. 2000–2008, Apr. 2014.

[66] E. Carrasco and J. Perruisseau-Carrier, "Reflectarray antenna at terahertz using graphene," *IEEE Antennas Wireless Propag. Lett.*, vol. 12, pp. 253–256, 2013.

[67] Z.-W. Miao, Z.-C. Hao, Y. Wang, B.-B. Jin, J.-B. Wu, and W. Hong, "A 400-GHz high-gain quartz-based single layered folded reflectarray antenna for terahertz applications," *IEEE Trans. THz Sci. Technol.*, vol. 9, no. 1, pp. 78–88, Jan. 2019.

[68] R. Deng, F. Yang, S. Xu, and M. Li, "A 100-GHz metal-only reflectarray for high-gain antenna applications," *IEEE Antennas Wireless Propag. Lett.*, vol. 15, pp. 178–181, 2016.

[69] Z.-W. Miao, Z.-C. Hao, and Q. Yuan, "Design and implementation of a G-Band silicon-based single-layer reflectarray antenna," *IEEE Antennas Wireless Propag. Lett.*, vol. 16, pp. 2191–2194, 2017.

[70] W. Lee and Y. J. Yoon, "A broadband Dual-Metallic-Reflectarray antenna for millimeter-wave applications," *IEEE Antennas Wireless Propag. Lett.*, vol. 16, pp. 856–859, 2017.

[71] K. Konstantinidis, A. P. Feresidis, and P. S. Hall, "Broadband sub-wavelength profile high-gain antennas based on multi-layer metasurfaces," *IEEE Trans. Antennas Propag.*, vol. 63, no. 1, pp. 423–427, Jan. 2015.

[72] Y.-H. Yu, W. Wu, Z.-Y. Zong, and D.-G. Fang, "A Wire-Metamaterial-Loaded resonant cavity antenna using 3-D printing technology," *IEEE Antennas Wireless Propag. Lett.*, vol. 17, no. 11, pp. 2119–2122, Nov. 2018.

[73] A. A. Baba, R. M. Hashmi, K. P. Esselle, and A. R. Weily, "Compact high-gain antenna with simple all-dielectric partially reflecting surface," *IEEE Trans. Antennas Propag.*, vol. 66, no. 8, pp. 4343–4348, Aug. 2018.

[74] A. Lalbakhsh, M. U. Afzal, K. P. Esselle, S. L. Smith, and B. A. Zeb, "Single-dielectric wideband partially reflecting surface with variable reflection components for realization of a compact high-gain resonant cavity antenna," *IEEE Trans. Antennas Propag.*, vol. 67, no. 3, pp. 1916–1921, Mar. 2019.

[75] F. Wu and K. M. Luk, "Circular polarization and reconfigurability of Fabry–Pérot resonator antenna through metamaterial-loaded cavity," *IEEE Trans. Antennas Propag.*, vol. 67, no. 4, pp. 2196–2208, Apr. 2019.

[76] F. Meng and S. K. Sharma, "A wideband resonant cavity antenna with compact partially reflective surface," *IEEE Trans. Antennas Propag.*, vol. 68, no. 2, pp. 1155–1160, Feb. 2020.
[77] M. Asaadi, I. Afifi, and A.-R. Sebak, "High gain and wideband high dense dielectric patch antenna using FSS superstrate for millimeter-wave applications," *IEEE Access*, vol. 6, pp. 38243–38250, 2018.
[78] H. Attia, M. L. Abdelghani, and T. A. Denidni, "Wideband and high-gain millimeter-wave antenna based on FSS Fabry–Perot cavity," *IEEE Trans. Antennas Propag.*, vol. 65, no. 10, pp. 5589–5594, Oct. 2017.
[79] Q.-Y. Guo and H. Wong, "A millimeter-wave Fabry–Pérot cavity antenna using fresnel zone plate integrated PRS," *IEEE Trans. Antennas Propag.*, vol. 68, no. 1, pp. 564–568, Jan. 2020.
[80] Q.-Y. Guo and H. Wong, "Wideband and high-gain Fabry–Pérot cavity antenna with switched beams for millimeter-wave applications," *IEEE Trans. Antennas Propag.*, vol. 67, no. 7, pp. 4339–4347, Jul. 2019.
[81] D. Abbou, T. P. Vuong, R. Touhami, F. Ferrero, D. Hamzaoui, and M. C. E. Yagoub, "High-gain wideband partially reflecting surface antenna for 60 GHz systems," *IEEE Antennas Wireless Propag. Lett.*, vol. 16, pp. 2704–2707, 2017.
[82] H. Attia, "Analytical prediction of the radiation characteristics of 2 × 2 ridge gap waveguide slot antenna array with suppressed grating lobes at the V-band," *IEEE Access*, vol. 7, pp. 95132–95139, 2019.
[83] C. Gu, S. Gao, B. Sanz Izquierdo, G. J. Gibbons, P. R. Young, E. A. Parker, F. Qin, G. Wen, Z. Cheng, Y. Geng, and Y. Liu, "Wideband high-gain millimetre/submillimetre wave antenna using additive manufacturing," *IET Microw., Antennas Propag.*, vol. 12, no. 11, pp. 1758–1764, Sep. 2018.
[84] A. P. Feresidis and J. C. Vardaxoglou, "High gain planar antenna using optimised partially reflective surfaces," *IEE Proc.-Microw., Antennas Propag.*, vol. 148, no. 6, pp. 345–350, 2001.

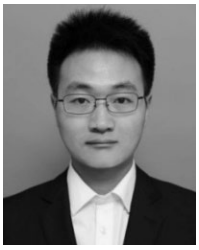

Rui Xu was born in Xi'an, China, in 1989. He received the B.E., master's, and Ph.D. degrees in electronic engineering from Northwestern Polytechnical University, Xi'an, in 2013, 2015, and 2018, respectively. Since 2019, he has been a Research Associate with the University of Kent. His current research interests include ultra-wideband linear and circularly polarization antennas, waveguide slot antenna arrays, THz antenna, print slot antennas, microstrip antennas, high gain antenna, and electromagnetic periodic structure.

STEVEN GAO received the Ph.D. degree in microwave engineering from Shanghai University, China. He is currently a Full Professor and the Chair of RF and microwave engineering, and the Director of Graduate Studies with the School of Engineering and Digital Arts, University of Kent, U.K. He has coauthored/co-edited three books, such as *Space Antenna Handbook* (Wiley, 2012), *Circularly Polarized Antennas* (IEEE-Wiley, 2014), and *Low-Cost Smart Antennas* (Wiley, 2019), over 300 articles and ten patents. His research interests include smart antennas, phased arrays, MIMO, reconfigurable antennas, wideband/multiband antennas, satellite antennas, RF/microwave/mm-wave/THz circuits, mobile communications, satellite communications, UWB radars, synthetic-aperture radars, the IoT, and sensors for healthcare. He is also a Fellow of Royal Aeronautical Society, U.K., and the IET, U.K. He was a General Chair of LAPC 2013, and an Invited Speaker at many conferences. He was a Distinguished Lecturer of IEEE AP Society. He is also an Associate Editor of the IEEE TRANSACTIONS ON ANTENNAS AND PROPAGATION and several other international journals, such as *Radio Science*, IEEE ACCESS, *Electronics Letters*, *IET Circuits, Devices & Systems*, and so on, and the Editor-in-Chief for John Wiley & Sons Book Series on Microwave and Wireless Technologies.

BENITO SANZ IZQUIERDO received the B.Sc. degree from ULPGC, Spain, and the M.Sc. and Ph.D. degrees from the University of Kent, U.K. He was a Research Associate with the School of Engineering, University of Kent, in 2013, became a Lecturer of electronic systems and, in 2018, a Senior Lecturer. In 2012, he worked for Harada Industries Ltd., where he developed novel antennas for the automotive industry. His research interests are multiband antennas, wearable electronics, additive manufacturing (3D printing), substrate integrated waveguides components, metamaterials, electromagnetic band-gap structures, frequency selective surfaces, and reconfigurable devices. He received awards and recognition for his work on wearable antennas (mention in the House of Lords, IEEE IWAT Best Paper Award), frequency selective surfaces (Best Paper at an IET workshop on Aerospace applications award), reconfigurable antennas (2017 CST University publication award for an IEEE Transactions paper) amongst others. His research has been funded through a variety of sources, such as the U.K. EPSRC, Royal Academy of Engineering, and the Royal Society.

CHAO GU received the B.S and M.S. degrees from Xidian University, Xi'an, China, in 2009 and 2012, respectively, and the Ph.D. degree from the University of Kent, Canterbury, U.K., in 2017. He is currently a Research Assistant with Queens University Belfast.

PATRICK REYNAERT (Senior Member, IEEE) was born in Wilrijk, Belgium, in 1976. He received the Master of Industrial Sciences degree in electronics (ing.) from the Karel de Grote Hogeschool, Antwerp, Belgium, in 1998, and the Master of Electrical Engineering (ir.) degree and the Ph.D. (dr.) degree in engineering science from the University of Leuven (KU Leuven), Leuven, Belgium, in 2001 and 2006, respectively. From 2006 to 2007, he was a Postdoctoral Researcher with the Department of Electrical Engineering and Computer Sciences, University of California at Berkeley, Berkeley, CA, USA, with the support of a BAEF Francqui Fellowship. In 2007, he was a Visiting Researcher with Infineon, Villach, Austria. Since October 2007, he has been a Professor with the Department of Electrical Engineering (ESAT-MICAS), KU Leuven. His current research interests include mm-wave and THz CMOS circuit design, high-speed circuits, and RF power amplifiers. Dr. Reynaert is also the Chair of the IEEE SSCS Benelux Chapter. He serves or has served on the Technical Program Committees of several international conferences, including ISSCC, ESSCIRC, RFIC, PRIME, and IEDM. He has served as an Associate Editor for the IEEE TRANSACTIONS ON CIRCUITS AND SYSTEMS—I: REGULAR PAPERS, and a Guest Editor for the IEEE JOURNAL OF SOLID-STATE CIRCUITS.

ALEXANDER STANDAERT (Student Member, IEEE) was born in Wilrijk, Belgium, in 1991. He received the B.Sc. and M.Sc. degrees in electronics engineering, from Katholieke Universiteit Leuven, Leuven, Belgium, in 2012 and 2014, respectively, where he is currently pursuing the Ph.D. degree in data communications through polymer waveguides. Since 2014, he has been a Research Assistant with MICAS, Katholieke Universiteit Leuven.

GREGORY J. GIBBONS received the Ph.D. degree from the Department of Physics, The University of Warwick. After time spent in the private sector, he returned to Warwick to join WMG in 1997 and has headed the AM group since 2001, providing excellence in research, teaching, and knowledge transfer of AM and related technologies. He is currently the Head of additive manufacturing (AM) with WMG. His research interests include new applications for AM, and development of next-generation AM technologies. He was appointed to a Reader at WMG in 2014, has over 20 years' experience in the field of AM, with >60 peer-reviewed publications, H-index 12. He has a wide portfolio of funded research, being principal investigator on a number of EPSRC, iUK, HVM Catapult, and industrially funded projects, including collaborations with UK and EU Universities, Research Organizations, and industry. His strong industrial engagement extends from SMEs through to OEMS (e.g., BAE Systems, Bombardier, Unilever, and AkzoNobel). Dr. Gibbons is a long standing Fellow of the Institute of Materials, Minerals, and Mining. He is the Co-Chair of the High Value Manufacturing Catapult AM Forum, promoting AM across the HVM Centres to industry. He is a Module Tutor for the Manufacturing Process Technology module, part of WMG's Manufacturing Systems and Management M.Sc. programme. In addition, he lectures on undergraduate programmes in the areas of AM and associated down-stream technologies, including Rapid Casting and Rapid Tooling.

WOLFGANG BÖSCH (Fellow, IEEE) joined the Graz University of Technology as a Professor in Austria to establish a new Institute for Microwave and Photonic Engineering, in 2010. One focus of the research group is on characterization, design and modeling of microwave, and mm-wave components and systems. Before joining Graz University of Technology, he has been the CTO of the Advanced Digital Institute in the U.K., a not for profit organization to promote research activities. He has also been the Director of Business and Technology Integration of RFMD (UK) Ltd. For almost ten years, he has been with Filtronic plc as the CTO of Filtronic Integrated Products and as the Director of the Global Technology Group mainly responsible for the technology road-mapping, strategy formulation, and the development of many innovative products.

MICHAEL ERNST GADRINGER (Member, IEEE) received the Dipl.-Ing. and Dr.Techn. degrees from the Vienna University of Technology, Austria, in 2002 and 2012, respectively. Since 2010, he has been a University Assistant with the Institute of Microwave and Photonic Engineering, Graz University of Technology, Austria. During his studies, he was involved with the design of analog and digital linearization systems for power amplifiers and with the behavioral modeling of microwave circuits. His current research activities focus on the design and linearization of broadband microwave and mm-wave communication systems as well as on mm-wave measurement techniques and de-embedding. He has coedited the book *RF Power Amplifier Behavioral Modeling* (Cambridge University Press).

DONG LI was born in Xi'an, China. He received the B.S. degree in electrical engineering from Northwestern Polytechnical University, in 2006, and the M.S. degree from Beihang University, in 2009. He has been a Visiting Researcher with the School of Engineering and Digital Arts, University of Kent, Canterbury, U.K. He is currently working as a Senior Engineer with the Xi'an Institute of Space Radio Technology (XISRT), Xi'an. His research interests include microwave/millimeter-wave antennas, reflectarray antennas, and phase array antennas.